

1 Attribution of direct ozone radiative forcing to
2 spatially resolved emissions

K. Bowman¹ and D. K. Henze²

K. Bowman, Jet Propulsion Laboratory, California Institute of Technology, 4800 Oak Grove
Dr., Pasadena, CA, 91109

D. Henze, Department of Mechanical Engineering, University of Colorado, 1111 Engineering
Drive, Boulder, CO 80309, USA.

¹California Institute of Technology, Jet
Propulsion Laboratory, Pasadena,
California, USA

²University of Colorado, Boulder,
Colorado, USA

3 Quantifying the dependence of ozone direct radiative forcing (DRF) on the
4 mixture and spatial distribution of precursor emissions is a key step towards
5 understanding the impact of air quality standards on climate. We use here
6 a combination of satellite observations of ozone and its radiative effect in con-
7 junction with an adjoint chemical transport model to determine the ozone
8 DRF due to global, anthropogenic NO_x , CO, and non-methane hydrocar-
9 bons (NMHC) emissions at $2^\circ \times 2.5^\circ$ regions. We show that 8% of the ozone
10 DRF from the sum of all these emissions can be attributed to 15 regions, which
11 are predominantly located in China and the US. To achieve an equivalent
12 reduction in ozone DRF, necessary emission reductions for each precursor
13 vary intra-continentally by a factor of 3-10 and globally by over an order of
14 magnitude. The contribution of NO_x emissions to ozone DRF relative to CO
15 and NMHC emissions within individual regions varies globally by nearly a
16 factor of two.

1. Introduction

17 Air quality and climate co-benefit strategies for ozone are complicated by the complex
18 spatio-temporal structure of tropospheric ozone and the non-linear chemistry relating
19 precursor emissions to ozone distributions [*Forster et al.*, 2007; *H. Levy II et al.*, 2008; *Sitch*
20 *et al.*, 2007; *Kawase et al.*, 2011]. Previous studies have focused on climate responses to
21 continental-scale radiative forcing (RF) [*Shindell and Faluvegi*, 2009], the role of sectorally
22 aggregated [*Unger et al.*, 2010; *Fuglestedt et al.*, 2008] and continental-scale [*Naik et al.*,
23 2005; *Berntsen et al.*, 2006; *Stevenson and Derwent*, 2009] changes in precursor emissions
24 on RF, and the degree to which increases in CH₄ radiative forcing following NO_x reductions
25 can offset reduced ozone direct radiative forcing [*Naik et al.*, 2005; *Fiore et al.*, 2008;
26 *Derwent et al.*, 2008; *Stevenson and Derwent*, 2009].

27 In this work we address the role of regional ($2^\circ \times 2.5^\circ$) variations in chemical environment
28 and transport in modulating direct ozone radiative forcing (DRF) at intra-continental
29 scales through a novel approach that uses satellite observations from the Tropospheric
30 Emission Spectrometer (TES) in conjunction with adjoint sensitivity analysis from the
31 GEOS-Chem chemistry and transport model. Observationally constrained radiative forc-
32 ings are calculated in each grid-cell for more than thirty different emission types, including
33 both natural and sector-specific anthropogenic O₃ precursors; we focus here on anthro-
34 pogenic NO_x, CO, and NMHC sources because of their dominant role in ozone photo-
35 chemistry and air quality (contributions of sector-aggregated NO_x emissions are provided
36 in Supplemental Table 1). This level of quantification is made feasible through the use
37 of an adjoint model, which in general is an efficient means of calculating sensitivities

with respect to large numbers of model inputs (in this case emissions). This approach, however, only accounts for ozone direct RF, which does not include methane-ozone feedbacks or indirect methane RF. These additional effects have a significant impact on total RF from precursor emissions and would need to be included in any comprehensive air quality-climate co-benefit analysis.

2. Methods

Tropospheric O₃ radiative effects using TES IRKs

The Tropospheric Emissions Spectrometer (TES) is a polar sun-synchronous, high resolution (0.1 cm⁻¹ apodized), infrared Fourier transform spectrometer aboard the NASA Aura satellite with a global repeat cycle of 16 days and an averaged nadir footprint of 5 km × 8 km [Beer, 2006]. Vertical ozone profiles are derived from spectrally-resolved top-of-the-atmosphere (TOA) thermal radiances based on an optimal estimation framework [Bowman *et al.*, 2006]. This relationship between TOA radiances and ozone distributions was first exploited to quantify the greenhouse gas effect of upper tropospheric ozone over clear-sky, oceanic scenes [Worden *et al.*, 2008] but was subsequently formalized for all-sky and land/oceans scenes through the introduction of longwave instantaneous radiative kernels (IRK) defined as

$$\mathbf{k}_i = \frac{\partial F_i}{\partial \mathbf{c}_i} \quad (1)$$

where F_i is the instantaneous upward TOA flux in atmospheric column location i integrated across the infrared band in W/m², \mathbf{c}_i is the TES retrieved ozone profile on L pressure levels, and \mathbf{k}_i is the IRK in W/m²/ppb of the i th column. Under clear-sky scenes,

46 the global mean IRK peak sensitivity for August 2006 is about $0.6 \text{ mW/m}^2/\text{ppb}$ at around
47 550 hPa, decreasing linearly in pressure towards the surface and the tropopause. TES
48 ozone and IRKs have been applied to chemistry climate model evaluation [*Aghedo et al.*,
49 2011a] and TES sampling has been shown to be sufficiently accurate to estimate zonal
50 monthly mean distributions to within a few ppb [*Aghedo et al.*, 2011b]. The unweighted
51 global mean of the all-sky longwave radiative effect, which includes both natural and an-
52 thropogenic ozone, is $0.33 \pm 0.02 \text{ W/m}^2$ [*Worden et al.*, 2011] . The longwave radiative
53 effect from TES is less than most estimates of the anthropogenic component (i.e., radia-
54 tive forcing) alone [*Forster et al.*, 2007]. These differences can be attributed in part to
55 definitions of radiative forcing, which is commonly defined at the tropopause, spans the
56 shortwave (SW) and long wave (LW) spectrums, and includes stratospheric temperature
57 adjustment. The SW is generally a small contribution to ozone RF. The instantaneous
58 TOA RF is about 10-20% higher than the stratospherically adjusted RF depending on
59 the model[*Forster et al.*, 2007].

GEOS-Chem forward and adjoint model

60 GEOS-Chem (www.geos-chem.org) is a chemical transport model primarily driven by
61 assimilated meteorology from the Goddard Earth Observing System (GEOS) of the NASA
62 Global Modeling and Assimilation Office (GMAO). The spatial resolution of the GEOS
63 meteorological fields are reduced to facilitate detailed simulation of tropospheric gas-
64 phase HO_x - NO_x -VOC chemistry [*Bey et al.*, 2001]. For this work, we use model v8-02-01
65 with relevant updates through v9-01-01, run at the global $2^\circ \times 2.5^\circ$ resolution. Global
66 anthropogenic emissions of NO_x are from EDGAR [*Olivier et al.*, 2001], overwritten by

67 regional inventories in specific areas [*van Donkelaar et al.*, 2008]. Monthly biomass burning
 68 emissions are from GFEDv2 [*van der Werf et al.*, 2009] and biofuel emissions from [*Yevich*
 69 *and Logan*, 2003]. The adjoint of GEOS-Chem [*Henze et al.*, 2007] solves a set of equations
 70 auxiliary to the forward chemical transport model in a manner that efficiently yields the
 71 gradient of a scalar forward model response function with respect to all model parameters
 72 simultaneously. The adjoint has been used for analyzing long-rang impacts on O₃ [*Zhang*
 73 *et al.*, 2009; *Walker et al.*, 2012] as well as O₃ assimilation [*Singh et al.*, 2011; *Parrington*
 74 *et al.*, 2012].

Ozone radiative forcing

We first define the mean area weighted observed outgoing TOA longwave radiative forcing:

$$\mathcal{J} = \frac{1}{A} \sum_i^N a_i F_i \quad (2)$$

where F_i is the i th of N TOA fluxes measured by the TES satellite. The product is weighted by the area of the model grid, a_i , and normalized by the total area, $A = \sum_i^N a_i$. The sensitivity of the mean TOA flux to emissions of each ozone precursor in each model grid cell is then

$$\boldsymbol{\lambda} = \nabla_{\mathbf{E}} \mathcal{J} \quad (3)$$

where \mathbf{E} is a vector of emissions from each species, sector and in each grid cell. Equation 3 is the direct ozone radiative forcing when \mathbf{E} is anthropogenic. λ_i , The sensitivity in Eq 3 can be calculated for any single observed TOA flux from TES, F_i (extension to the global

mean TOA flux, \mathcal{J} , is straightforward) as

$$\lambda^i = \frac{a_i}{A} \frac{\partial F_i}{\partial \mathbf{E}} = \frac{a_i}{A} \left(\frac{\partial \mathbf{c}_i}{\partial \mathbf{E}} \right)^T \frac{\partial F_i}{\partial \mathbf{c}_i}, \quad (4)$$

75 where the chain rule is employed to separate the sensitivity of flux to concentrations
 76 and the sensitivity of concentrations to emissions. The product of the two terms on the
 77 far right hand of Eq. 4 is calculated by the adjoint model (see *Henze et al.* [2007]). The
 78 novelty of our approach is to use the observationally derived TES IRK's (Eq. 1) to quantify
 79 the derivative of the observed flux with respect to retrieved ozone profiles, and to then
 80 propagate this sensitivity efficiently backwards in time using an adjoint model to obtain
 81 sensitivities with respect to emissions. The adjoint sensitivities of the August DRF are
 82 integrated backwards through the beginning of July, by which time they asymptotically
 83 approach steady state values owing to the lifetime of tropospheric O₃. As shown in Figure
 84 S1 (Supplemental), adjoint estimates for ozone DRF from the emissions in individual grid
 85 cells are in consistent agreement with evaluation of the full forward model across a wide
 86 range of perturbations with a slope of 0.991 and R²=0.993, and the adjoint-based forcings
 87 are additive for modest changes to emissions across broader scales.

3. Results

88 The sensitivities of the outgoing longwave radiation at the top-of-the-atmosphere (TOA)
 89 as observed by TES with respect to spatially-resolved anthropogenic NO_x, CO, and NMHC
 90 emissions are shown in Fig. 1. These global emissions are defined on a 2°×2.5° grid, which
 91 we refer to as “regions.” We note that this observationally derived radiative forcing at
 92 the TOA is significantly lower [*Worden et al.*, 2008] than typical values modeled at the
 93 tropopause [*Forster et al.*, 2007]. We have focused on August, 2006, which is the sea-

94 sonal maximum in ozone radiative forcing for North America and consequently represents
95 the strongest diversity of forcing responses to emissions [Naik *et al.*, 2005]. There are
96 15 $2^\circ \times 2.5^\circ$ regions with a combined radiative forcing greater than 0.15 mW/m^2 , which
97 represents about 8% of ozone DRF from all anthropogenic emissions. For brevity, we
98 denote these $2^\circ \times 2.5^\circ$ regions by the names of the major city contained therein. Regions
99 within China accounts for 10 of these and includes the Shanghai region, which is globally
100 the most important: 0.31 (0.20 (NO_x), 0.07 (CO), 0.04 (NMHC)) mW/m^2 . While NO_x
101 emissions are usually the dominant radiative forcing in any single location, the Henan
102 province centered near Zhoukou (34°N , 115°E) is distinguished by a larger impact of
103 CO and NMHC (56%) versus NO_x emissions (44%) to its total radiative forcing of 0.16
104 mW/m^2 . The United States contribution includes Houston 0.17 (0.12 (NO_x), 0.02 (CO),
105 0.03 (NMHC)), New Orleans 0.16 (0.12 (NO_x), 0.02 (CO), 0.02 (NMHC)), and Western
106 Atlanta 0.16 (0.11 (NO_x), 0.02 (CO), 0.02 (NMHC)). The remaining regions are Mexico
107 City 0.27 (0.16 (NO_x), 0.04 (CO), 0.07 (NMHC)) and Kuala Lumpur 0.15 (0.13 (NO_x),
108 0.01 (CO), 0.01 (NMHC)). The impact of these latter regions is accentuated by their
109 efficient transport pathways to the upper troposphere. Consistent with previous studies
110 [Naik *et al.*, 2005], high latitude regions, such as in Europe, play a minor role in direct
111 ozone radiative forcing despite having comparable emission levels.

112 The heterogeneity in ozone DRF for August 2006 as shown in Fig. 1 is a function of
113 several factors: the season, the magnitude of the underlying emissions in each grid-cell,
114 the photochemical efficiency of O_3 formation in a given location per amount of precursor
115 emitted, the transport of ozone into the free troposphere and the underlying distribution

116 of clouds, water vapour, and temperature. In order to isolate the role of the physical
117 atmospheric structure relative to the emission magnitude, we define a radiative forcing
118 efficiency ($r_{eff}(x, y)$) as a ratio of the global mean ozone DRF sensitivity for a single
119 emission location to the global mean ozone sensitivity to that same emission location. If,
120 for example, changing NO_x emissions for a location by 100% leads to a 0.1% change in
121 global mean ozone and a 0.125% change in global mean ozone DRF, then $r_{eff} = 1.25$.

122 A plot of this radiative forcing efficiency is shown in Fig. 2 for NO_x emissions. Differences
123 are particularly striking between North America and Europe, with NO_x emissions from the
124 former producing O_3 that is nearly twice as radiatively efficient. The meridional effect in
125 radiative forcing efficiency [Naik *et al.*, 2005] leads to a maximum in the tropics, decreasing
126 poleward by over a factor of two. In general, this ratio is highest in areas with convective
127 lofting (i.e., the tropics) and over regions of higher altitude. However, there are important
128 zonal variations that are related to cloud cover and convection. For example, r_{eff} is high
129 (> 1.2) over Saudi Arabia and Iran for August 2006 because surface temperatures are both
130 very high and the regions are relatively cloud free. Changes in atmospheric circulation
131 due to monsoons have a significant impact on the export of surface emissions to the free
132 troposphere. The highest values of r_{eff} are due to the Western African Monsoon, which
133 is related to the shift of the inter-tropical convergence zone northward from the tropical
134 Atlantic ocean towards the Saharan desert. The strong poleward temperature gradient
135 results in a complex circulation pattern leading to significant convection and export along
136 both mid-level African and high-level Tropical Easterly Jets [Savidge *et al.*, 2007]. The
137 onset of the Indo-Australian Monsoon is influenced by El Niño conditions and a complex

138 air-land interaction [Moron *et al.*, 2009], but the region is convectively unstable for all
139 seasons leading to a very high r_{eff} . Radiative forcing efficiencies of CO and NMHCs,
140 which are available in Supplemental Fig. S2, have the same meridional gradient but a
141 much more diffuse zonal distribution.

142 The variability of r_{eff} on spatial resolutions at which air quality strategies are enacted
143 in practice has important policy implications. To illustrate the potential of this approach
144 for supporting policy analysis, $2^\circ \times 2.5^\circ$ regions with approximately the same total DRF,
145 i.e., the DRF from the sum of NO_x , CO, and NMHC emissions, of 0.1 ± 0.01 mW/m² are
146 shown in Fig. 3 (details shown in supplemental Table 2).

147 Across the 27 regions matching this criteria, NO_x emissions represent about $64 \pm 14\%$ of
148 the DRF. Emissions increase with latitude by roughly a factor of 5-20 depending on the
149 precursor emissions with considerable zonal scatter. For example, the Guatemala City
150 region has 10 times smaller NO_x emissions than Chicago and almost 20 times lower CO
151 emissions than Beijing but has approximately the same total DRF. Similarly, the Brunei
152 region near Malaysia has 5 times lower NMHC emissions than the Philadelphia region.
153 These variations are driven by the poleward temperature gradient as well as cloud cover
154 and large scale processes such as the Asian monsoon. Continental scale processes lead to
155 a considerable spread in emissions as well. The region east of Atlanta (not to be confused
156 with the Western Atlanta region discussed previously) has the lowest NO_x emissions of the
157 11 United States regions and is 3.5 times lower than Chicago. The enhanced sensitivity
158 in the Southeastern US is associated with summertime convection [Li *et al.*, 2005], as
159 shown by r_{eff} in the supplemental Fig. S3. Consequently, the variability of US emissions

160 with 0.1 mW/m^2 DRF is about half of the mean: $4.3 \pm 2.1(\text{NO}_x)$, 21 ± 12 (CO), and
161 1.7 ± 1.0 (NMHC) $\text{Mg/km}^2/\text{yr}$. The choice of metrics used in an air-quality climate co-
162 benefit analysis could lead to very different results based on this variability. For example,
163 a 10% reduction in NO_x emissions in Chicago would lead to 0.01 mW/m^2 change in
164 DRF but the equivalent absolute reduction to emissions east of Atlanta would lead to a
165 0.035 mW/m^2 DRF reduction. Consequently, controlling against emissions for air quality
166 versus DRF for climate can lead to very different strategies depending on location. It is
167 important to identify various approaches to attaining the targeted O_3 DRF as reductions
168 in NO_x emissions will increase methane lifetime—a more efficient greenhouse gas—whereas
169 reductions in CO and NMHC will decrease methane lifetime [West *et al.*, 2006].

170 The accuracy of grid-scale radiative forcings is limited by a knowledge of precursor
171 emission distributions and their ozone response, tracer transport, and the distribution of
172 clouds. Nevertheless, such results can be aggregated and compared to previous studies.
173 While the magnitude of the infrared, top-of-the-atmosphere ozone DRF reported here
174 is smaller from ozone DRF defined at the tropopause by a factor of six, the relative
175 sensitivity of ozone DRF to fractional emission changes aggregated to continental scales
176 closely follows that of a previous work [Naik *et al.*, 2005] using different model emissions,
177 chemistry and transport (see supplemental Fig. S4). The agreement in relative sensitivity
178 suggests that the differences are due to satellite versus model calculation of the ozone
179 radiative effect rather than linearity assumptions in the adjoint approach.

4. Conclusion

180 Overall, we have shown here that there is substantial variability in the radiative forcing
181 of O₃ precursor emissions at regional scales, and that the combined use of remote sensing
182 observations and adjoint modeling provides a means of characterizing such variability.
183 Further, there is considerable variability in the extent to which different precursors (NO_x
184 vs CO vs hydrocarbons) contribute to ozone's radiative impacts, as well as variability in
185 the contribution of different emissions sectors within these species, which are critical for
186 the overall O₃ response to emissions changes when accounting for the full range of chemical
187 and physical feedbacks. Incorporation of climate co-benefits into air quality mitigation
188 strategies thus requires quantitative understanding of chemical and physical processes at
189 scales ranging from sub-continental to global.

190 Equally important as design of control strategies is a framework to observe and assess
191 the efficacy of these strategies against the backdrop of natural variability. While we do
192 not address this framework explicitly, the satellite observations and assimilation system
193 used in this study would be essential elements. The proposed suite of geo-stationary com-
194 position satellites from the Atmospheric Composition Constellation (ACC) as part of the
195 Committee on Earth Observing Satellites (CEOS) (<http://www.ceos.org>) in conjunction
196 with surface measurements could potentially provide the necessary observing system to
197 support the implementation of ozone climate mitigation strategies. The requirements for
198 such as system will be a point of future research.

199 **Acknowledgments.** We would like thank Helen Worden (NCAR) and the
200 TES team for the IRK products. We acknowledge sponsorship from NASA

201 AQUEST (NNH09ZDA001N), AURA (NNH07ZDA001N), New Investigator program
202 (NNH09ZDA001N) and HEC computing facilities.

References

- 203 Aghedo, A. M., et al. (2011a), The vertical distribution of ozone instantaneous radiative
204 forcing from satellite and chemistry climate models, *J. Geophys. Res.-Atmos.*, *116*,
205 D01305, doi:10.1029/2010JD014243.
- 206 Aghedo, A. M., K. W. Bowman, D. T. Shindell, and G. Faluvegi (2011b), The impact
207 of orbital sampling, monthly averaging and vertical resolution on climate chemistry
208 model evaluation with satellite observations, *Atmos. Chem. Phys.*, *11*(13), 6493–6514,
209 doi:10.5194/acp-11-6493-2011.
- 210 Beer, R. (2006), TES on the Aura mission: Scientific objectives, measurements, and
211 analysis overview, *IEEE Trans. on Geosci. Remote Sensing*, *44*(5), 1102–1105.
- 212 Berntsen, T., J. Fuglestedt, G. Myhre, F. Stordal, and T. Berglen (2006), Abatement
213 of greenhouse gases: Does location matter?, *Climatic Change*, *74*(4), 377–411, doi:
214 10.1007/s10584-006-0433-4.
- 215 Bey, I., et al. (2001), Global modeling of tropospheric chemistry with assimilated meteo-
216 rology: Model description and evaluation, *J. Geophys. Res.-Atmos.*, *106*(D19), 23,073–
217 23,095.
- 218 Bowman, K. W., et al. (2006), Tropospheric emission spectrometer: Retrieval
219 method and error analysis, *IEEE Trans. on Geosci. Remote Sensing*, *44*(5), doi:
220 10.1109/TGRS.2006.871234.

- 221 Derwent, R., D. Stevenson, R. Doherty, W. Collins, M. Sanderson, and C. Johnson (2008),
222 Radiative forcing from surface NO_x emissions: spatial and seasonal variations, *Climatic*
223 *Change*, *88*(3), 385–401, doi:10.1007/s10584-007-9383-8.
- 224 Fiore, A. M., J. J. West, L. W. Horowitz, V. Naik, and M. D. Schwarzkopf (2008), Charac-
225 terizing the tropospheric ozone response to methane emission controls and the benefits
226 to climate and air quality, *J. Geophys. Res.*, *113*, D08307, doi:10.1029/2007JD009162.
- 227 Forster, P., et al. (2007), Changes in Atmospheric Constituents and in Radiative Forcing,
228 in: Climate Change 2007: The Physical Science Basis. Contributions of working group I
229 to the fourth Assessment Report on the Intergovernmental Panel on Climate Change,
230 edited by Solomon, S., Wuin, D., Manning, M., Chen, A., Marquis, M., Averyt, K.,
231 Tignor, M., and Miller, H., Cambridge University Press, Cambridge, United Kingdom
232 and New York, NY, USA, *Tech. rep.*, aR4.
- 233 Fuglestvedt, J., T. Berntsen, G. Myhre, K. Rypdal, and R. B. Skeie (2008), Climate
234 forcing from the transport sectors, *Proc. Natl. Acad. Sci. U. S. A.*, *105*(2), 454–458,
235 doi:10.1073/pnas.0702958104.
- 236 H. Levy II, M. D. Schwarzkopf, L. Horowitz, V. Ramaswamy, and K. L. Findell (2008),
237 Strong sensitivity of late 21st century climate to projected changes in short-lived air
238 pollutants, *J. Geophys. Res.*, *113*, D06102, doi:10.1029/2007JD009176.
- 239 Henze, D. K., A. Hakami, and J. H. Seinfeld (2007), Development of the adjoint of GEOS-
240 Chem, *Atmos. Chem. Phys.*, *7*, 2413–2433.
- 241 Kawase, H., T. Nagashima, K. Sudo, and T. Nozawa (2011), Future changes in tropo-
242 spheric ozone under Representative Concentration Pathways (RCPs), *Geophys. Res.*

243 *Lett.*, 38(5).

244 Li, Q., D. J. Jacob, R. Park, Y. Wang, C. L. Heald, R. Hudman, R. M. Yantosca, R. V.
245 Martin, and M. Evans (2005), North American pollution outflow and the trapping of
246 convectively lifted pollution by upper-level anticyclone, *J. Geophys. Res.*, 110, D10301,
247 doi:10.1029/2004JD005039.

248 Moron, V., A. W. Robertson, and R. Boer (2009), Spatial coherence and seasonal pre-
249 dictability of monsoon onset over Indonesia, *Journal of Climate*, 22(3), 840–850, doi:
250 10.1175/2008JCLI2435.1.

251 Naik, V., D. Mauzerall, L. Horowitz, M. D. Schwarzkopf, V. Ramaswamy, and M. Op-
252 penheimer (2005), Net radiative forcing due to changes in regional emissions of
253 tropospheric ozone precursors, *J. Geophys. Res.-Atmospheres*, 110, D24306, doi:
254 10.1029/2005JD005908.

255 Olivier, J. G. J., J. J. M. Berdowski, J. A. H. W. Peters, J. Bakker, A. J. H. Visschedijk,
256 and J. P. J. Bloos (2001), Applications of EDGAR including a description of EDGAR
257 3.2: reference database with trend data for 1970-1995, *RIVM report 773301 001/NRP*
258 *report 410200 051*, pp. RIVM, Bilthoven.

259 Parrington, M., et al. (2012), The influence of boreal biomass burning emissions on the
260 distribution of tropospheric ozone over North America and the North Atlantic during
261 2010, *Atmos. Chem. Phys.*, 12(4), 2077–2098, doi:10.5194/acp-12-2077-2012.

262 Sauvage, B., F. Gheusi, V. Thouret, J. P. Cammas, J. Duron, J. Escobar, C. Mari,
263 P. Mascart, and V. Pont (2007), Medium-range mid-tropospheric transport of ozone
264 and precursors over Africa: two numerical case studies in dry and wet seasons, *Atmos.*

- 265 *Chem. Phys.*, 7(20), 5357–5370, doi:10.5194/acp-7-5357-2007.
- 266 Shindell, D., and G. Faluvegi (2009), Climate response to regional radiative forcing during
267 the twentieth century, *Nature Geoscience*, 2(4), 294–300, doi:10.1038/ngeo473.
- 268 Singh, K., M. Jardak, A. Sandu, K. Bowman, M. Lee, and D. Jones (2011), Construction
269 of non-diagonal background error covariance matrices for global chemical data assim-
270 lation, *Geosci. Model Dev.*, 4(2), 299–316, doi:10.5194/gmd-4-299-2011.
- 271 Sitch, S., P. M. Cox, W. J. Collins, and C. Huntingford (2007), Indirect radiative forc-
272 ing of climate change through ozone effects on the land-carbon sink, *Nature*, doi:
273 10.1038/nature06059.
- 274 Stevenson, D. S., and R. G. Derwent (2009), Does the location of aircraft nitrogen
275 oxide emissions affect their climate impact?, *Geophys. Res. Lett.*, 36, L17810, doi:
276 10.1029/2009GL039422.
- 277 Unger, N., T. C. Bond, J. S. Wang, D. M. Koch, S. Menon, D. T. Shindell, and S. Bauer
278 (2010), Attribution of climate forcing to economic sectors, *Proc. Natl. Acad. Sci. U. S.*
279 *A.*, 107(8), 3382–3387, doi:10.1073/pnas.0906548107.
- 280 van der Werf, G. R., D. C. Morton, R. S. DeFries, L. Giglio, J. T. Randerson, G. J. Collatz,
281 and P. S. Kasibhatla (2009), Estimates of fire emissions from an active deforestation
282 region in the southern Amazon based on satellite data and biogeochemical modelling,
283 *Biogeosciences*, 6(2), 235–249.
- 284 van Donkelaar, A., et al. (2008), Analysis of aircraft and satellite measurements from the
285 Intercontinental Chemical Transport Experiment (INTEX-B) to quantify long-range
286 transport of East Asian sulfur to Canada, *Atmospheric Chemistry and Physics*, 8(11),

- 287 2999–3014, doi:10.5194/acp-8-2999-2008.
- 288 Walker, T. W., et al. (2012), Impacts of midlatitude precursor emissions and local photo-
289 tochemistry on ozone abundances in the Arctic, *J. Geophys. Res.*, *117*(D1), D01,305,
290 doi:10.1029/2011JD016370.
- 291 West, J. J., A. M. Fiore, L. W. Horowitz, and D. L. Mauzerall (2006), Global health
292 benefits of mitigating ozone pollution with methane emission controls, *Proc. Natl. Acad.*
293 *Sci. U. S. A.*, *103*(11), doi:10.1073/pnas.0600201103.
- 294 Worden, H. M., K. W. Bowman, J. R. Worden, A. Eldering, and R. Beer (2008), Satel-
295 lite measurements of the clear-sky greenhouse effect from tropospheric ozone, *Nature*
296 *Geoscience*, *1*(5), 305–308, doi:10.1038/ngeo182.
- 297 Worden, H. M., K. W. Bowman, S. S. Kulawik, and A. M. Aghedo (2011), Sensitivity of
298 outgoing longwave radiative flux to the global vertical distribution of ozone characterized
299 by instantaneous radiative kernels from Aura-TES, *J. Geophys. Res.*, *116*(D14), doi:
300 10.1029/2010JD015101.
- 301 Yevich, R., and J. A. Logan (2003), An assessment of biofuel use and burning of agri-
302 cultural waste in the developing world, *Global Biogeochem. Cycles*, *17*(4), 1095, doi:
303 10.1029/2002GB001952.
- 304 Zhang, L., D. J. Jacob, M. Kopacz, D. K. Henze, K. Singh, and D. A. Jaffe (2009), Inter-
305 continental source attribution of ozone pollution at western US sites using an adjoint
306 method, *Geophys. Res. Lett.*, *36*, L11810, doi:10.1029/2009gl037950.

Figure 1. Ozone direct radiative forcing (DRF), λ_{σ} , as attributed from TES observations for August 2006 to (a) NO_x emissions (b) CO emissions (scaled by 3) and (c) NMHC emissions (scaled by 3). The color scale is saturated for $\text{DRF} > 0.12 \text{ mW/m}^2$.

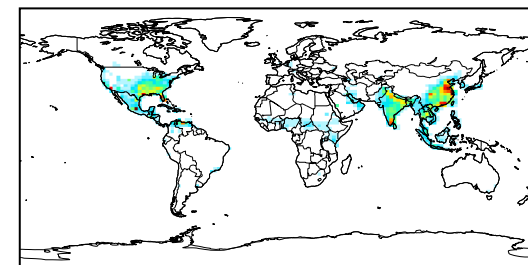
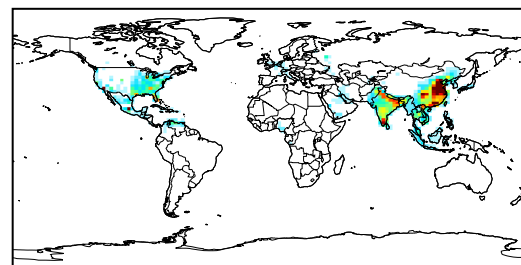
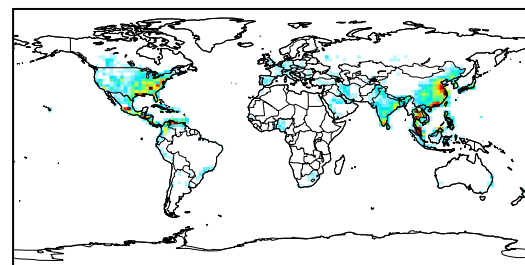
Figure 2. The impact of NO_x emission locations on ozone DRF. Areas where the radiative effectiveness ratio, r_{eff} , is greater (less) than one indicate regions where additional NO_x emissions would lead to an amplified (diminished) mean global ozone radiative forcing relative to the change in mean global ozone.

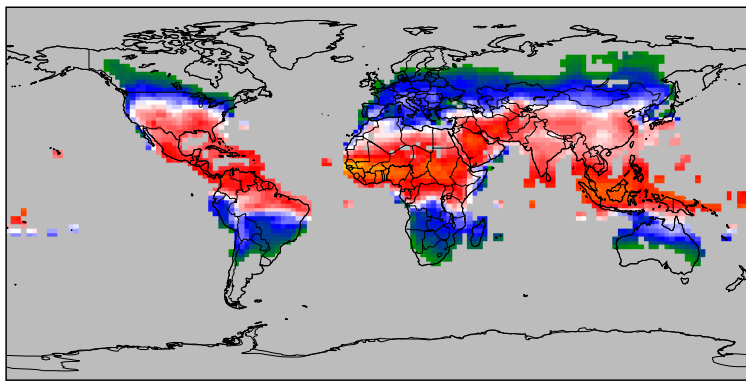
Figure 3. NO_x (black), CO (red), and NMHC (green) emissions that have about $0.1 \pm 0.01 \text{ mW/m}^2$ DRF. CO emissions have been reduced by 10 to fit on the same scale. Selected cities represent $2^\circ \times 2.5^\circ$ metropolitan regions and are identified adjacent to their respective emissions.

(a) NO_x

(b) $\text{CO} (\times 3)$

(c) NMHCs ($\times 3$)





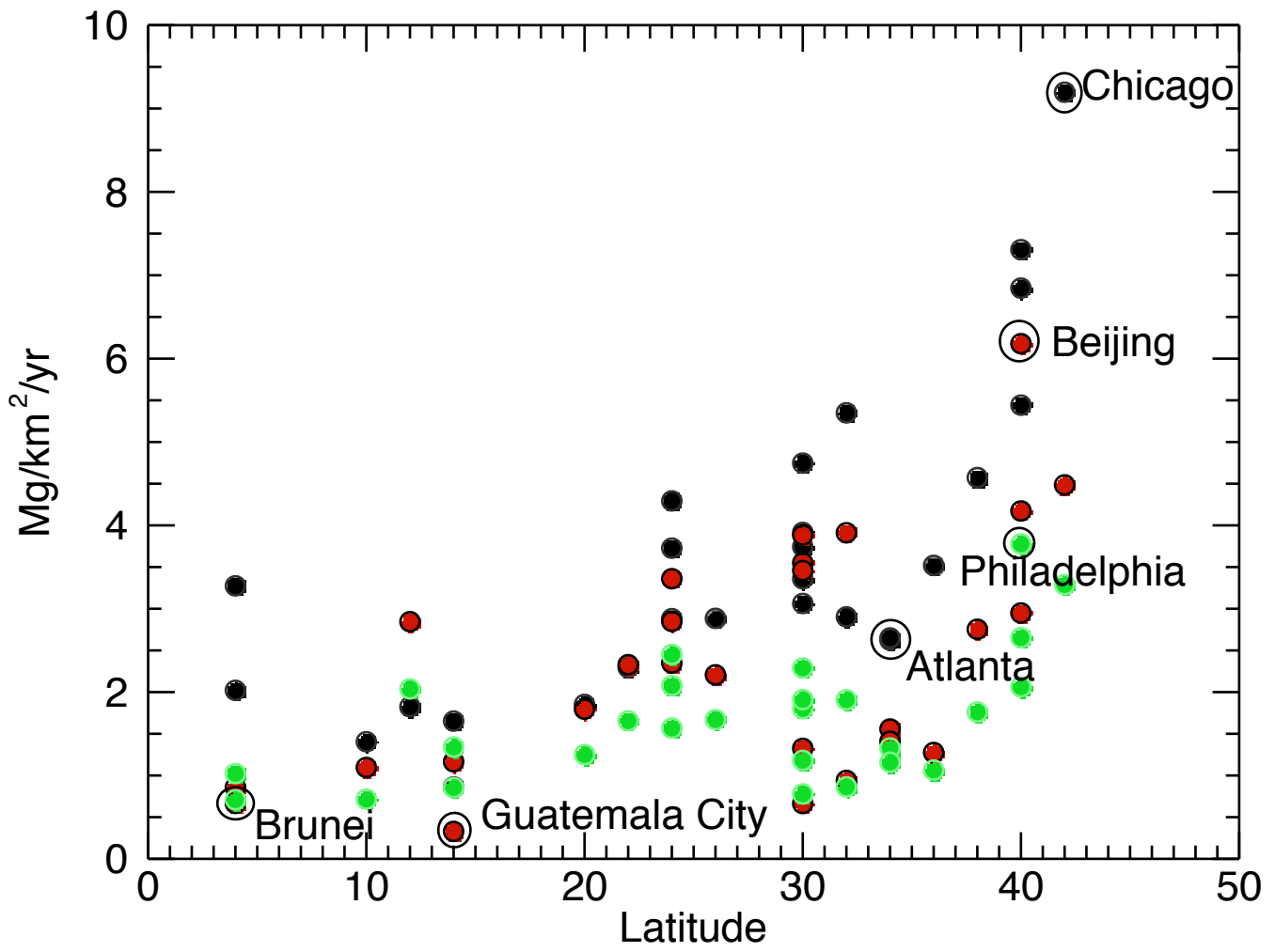
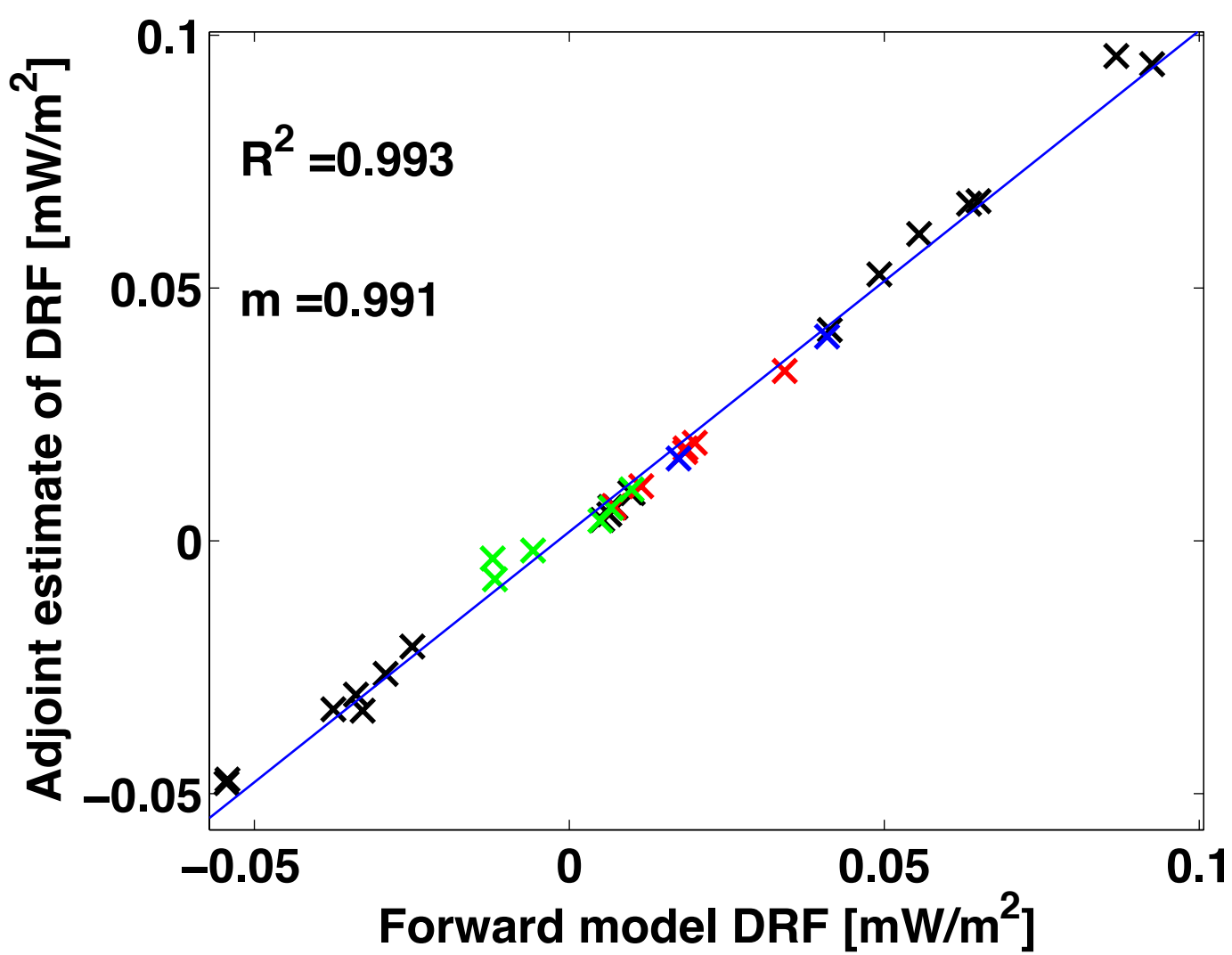


Figure S1: Validation of the ozone DRF from single-grid cell perturbations of NO_x (black), CO (red) and isoprene (green) emissions estimated using adjoint model sensitivities via comparison with the forward model estimates. Slope (m), fit line and R² for a linear regression are indicated on the plot. Included are -50%, 10%, and 100% perturbations for emissions of NO_x and 100% perturbations for emissions of CO and isoprene. Also shown (blue) are simultaneous perturbations to CO (100%) and NO_x (10%) compared to the sum of the adjoint based estimates for the ozone DRF of these emissions separately.

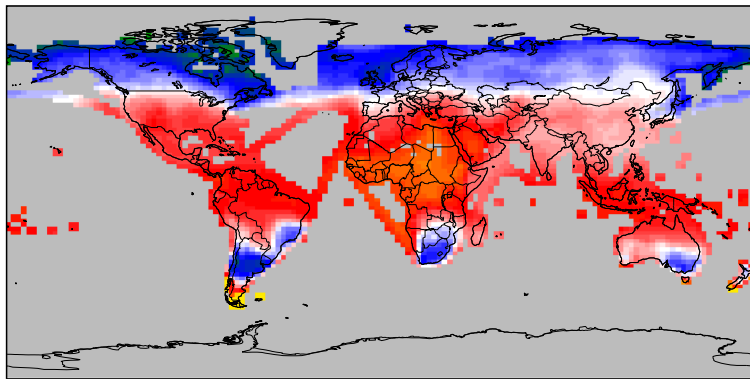
Figure S2: The impact of (a) CO emission and (b) NMHC emission locations on ozone DRF. Areas where the radiative effectiveness ratio, $reff$, is greater (less) than one indicate regions where additional CO emissions would lead to an amplified (diminished) mean global ozone radiative forcing relative to the change in mean global ozone.

Figure S3: The impact of North American NO_x emission locations on ozone DRF, which is the same as Fig. 3. Areas where the radiative effectiveness ratio, $reff$, is greater (less) than one indicate regions where additional NO_x emissions would lead to an amplified (diminished) mean global ozone radiative forcing relative to the change in mean global ozone.

Figure S4: Comparison between the results from the present manuscript (blue) and those of Naik et al. [2005] (red) for August. The panels show the following by region i: (a) global radiative forcings for a 10% perturbation to fossil fuel NO_x in region i and (b) these radiative forcings normalized by the total DRF summed across all regions from panel (a). The nine regions as defined in Naik et al. [2005] are: Africa and the Mid. East (AF), Australia (AU), East Asia (EA), Former Soviet Union (FSU), India (IN), North America (NA), South America (SA), and SE Asia (SE). The relative ordering between the regions is in remarkable agreement between the two studies, indicating that even though IRK-based estimates of O₃ radiative effects are on a different absolute basis than commonly considered, the relative distribution of the radiative forcing efficiencies, such as shown in Fig. 2, are likely to be more broadly applicable.



(a) CO



(b) NMHCs

